

Application of a Novel Fiber Surface Treatment Method in Fiber-reinforced Shells for Investment Casting

Zhicheng Feng¹, *Kai Lü^{1, 2, 3}, Lei Che¹, Xinyu Li¹

- 1. School of Materials Science and Engineering, Inner Mongolia University of Technology, Hohhot 010051, China;
- 2. Engineering Research Center of Development and Processing Protection of Advanced Light Metals, Ministry of Education, Hohhot, China; 3. The Inner Mongolia Advanced Materials Engineering Technology Research Center, Hohhot, China;

*Corresponding address: e-mail: nmglk83@imut.edu.cn

Abstract: To enhance the interfacial bonding between steel fibers and the shell, a novel fiber surface treatment method was proposed. SiO₂ nanoparticles were attached to fiber surfaces via a mechanical coating technique. At the microscale, FTIR was employed to analyze the functional groups on the fiber surfaces, followed by SEM to characterize the distribution of SiO₂ nanoparticles, and the fiber-shell interfacial bonding. At the macroscale, an orthogonal experimental design with (L₉(4³)) was adopted to optimize the process parameters. The bending strength and high-temperature self-load deformation of the reinforced shells were systematically evaluated. The results indicated that, the fiber treatment method is as follows: the weight ratio of fibers to SiO₂ nanoparticles is 1: 1, the ball milling speed is 400 r/min, the ball milling time is 10 min, and the addition amount is 0.15%. Under these conditions, the performance of the shell is the best. At this time, the green bending strength of the shell is 3.76 MPa, which is 86% higher than that without adding fibers. After calcination, the sintering bending strength is 6.83 MPa, which is 67% higher than that without adding fibers. The high-temperature bending strength is 18.22 MPa, and the high-temperature self-load deformation is 0.52%. The mechanical coating technique effectively deposited SiO₂ nanoparticles onto the fiber surfaces. The -OH introduced SiO₂ nanoparticles improved the interfacial wettability between fibers and the silica sol. And interactions between Si-O-H groups on the fiber surface and Si-O-H in the sol facilitated the formation of Si-O-Si covalent bonds, thereby strengthening the fiber-matrix interfacial adhesion. However, remain insufficiently understood and require further mechanistic investigation.

Keywords: investment casting; fiber-reinforced shell; mechanical coating technique; fiber surface treatment

1 Introduction

Investment casting (IC) enables the production of high-dimensional-accuracy complex near-net-shape, components, making it widely applicable in aerospace and advanced manufacturing sectors[1-4]. However, silica sol shells, a critical material in this process, face challenges such as low green bending strength and prolonged production cycles^[5-7]. The application of fiber-reinforced composite shell technology offers a promising solution to these limitations. Incorporating fibers into the shell matrix enhances both mechanical strength and gas permeability^[8-11]. Nevertheless, two critical issues remain unresolved: improving the distributive uniformity of fibers within the matrix to prevent agglomeration, and enhancing the interfacial bonding strength between fibers and the silica sol-based matrix, which directly governs load transfer efficiency and structural integrity under thermal-mechanical stresses^[12, 13].

The combination of fibers and interfaces can be classified into chemical bonding, adsorption and wetting, mechanical interlocking, and electrostatic interaction. Based on the interaction mechanism between fibers and shells, active functional groups can be introduced on the fiber surface to increase the surface free energy and generate chemical bonding^[14]. Or, the surface roughness of the fibers can be increased or the specific surface area can be enlarged to form mechanical interlocking with the shell^[15]. However, the surface of steel fibers is already very rough, and the large surface friction force makes the fibers prone to entanglement. Therefore, surface treatment of steel fibers is needed to introduce functional groups to improve the interface bonding. It is worth noting that steel fibers themselves do not have active functional groups and show chemical inertness, making them difficult to process^[16].

Zinc phosphate was initially applied as a modifying



agent for steel fiber surface treatment^[17]. However, its phosphorus (P) and zinc (Zn) components pose significant environmental risks, including heavy metal contamination and ecosystem toxicity. Subsequently, silane coupling agents-widely used for non-metallic fibers—were adapted for steel fibers, albeit requiring alkaline pretreatment to introduce high-density hydroxyl (-OH) groups onto the fiber surfaces. In fiber-reinforced shells, surface modification of fibers typically aims to graft hydroxyl groups that chemically bond with the silica sol matrix, which similarly necessitates complex chemical grafting procedures^[18, 19]. In contrast, this study proposes a novel fiber surface treatment method utilizing the adsorptive properties of SiO₂ nanoparticles combined with mechanical impingement to anchor them onto steel fiber surfaces. This approach addresses the tediousness of conventional chemical grafting while achieving superior interfacial bonding strength.

2 Materials and experimental methods

2.1 Mechanical Coating Technique

SiO₂ nanoparticles exhibit strong adsorption capabilities due to their high specific surface area. However, this characteristic also renders them prone to agglomerate spontaneously without external force, preventing direct adhesion to fiber surfaces. To address this limitation, a ball milling-assisted mechanical coating method was employed in this study. As illustrated in Fig. 1, the mechanical impingement generated by grinding balls facilitates direct contact between SiO₂ nanoparticles and fibers, enabling uniform deposition of nanoparticles onto fiber surfaces. This process effectively overcomes van der Waals forces-induced agglomeration while achieving controlled surface modification through tunable milling parameters.

The fiber material is 316L stainless steel (Fujian Qiangwen New Materials Co., Ltd., China), with a length of 4 mm and a diameter of 10 µm. The surface treatment is carried out by mechanical coating method, so that the SiO₂ nanoparticles (15 nm, Shanghai Yingcheng New Materials Co., Ltd., China) are attached to the surface of the fibers. The experimental device is a double-tank high-energy oscillating ball mill (MSK-SFM-3-11, Hefei mechanically stirred for 2 hours to form a stable slurry. The prepared slurries were then smearing to wax patterns fabricated using metal molds, followed by sand stuccoing and controlled drying. After completing the shell, dewaxing was performed to obtain shell specimens. In addition to room-temperature testing, selected specimens underwent sintering in a muffle furnace under the

Kexing Materials Technology Co., Ltd., China). The fibers and SiO₂ nanoparticles are added to the stainless steel mixing tank (80 ml, Hefei Kexing Materials Technology Co., Ltd., China) in a certain proportion. The total weight of the fibers and SiO₂ nanoparticles is 2 g, and the weight of the stainless steel grinding balls (Hefei Kexing Materials Technology Co., Ltd., China) is 25 g. The ratio of balls to materials is 25:2.

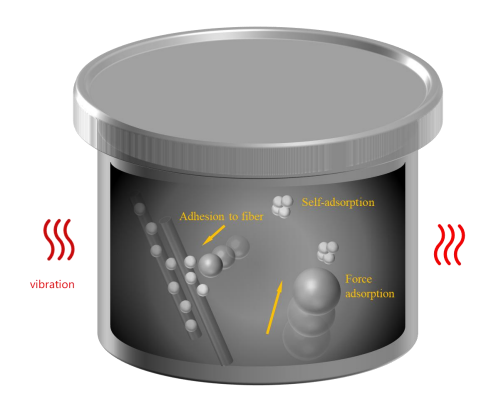


Fig. 1 Mechanical Coating Technique

2.2 Orthogonal Experimental Design

The critical parameters influencing the surface treatment efficacy include the fiber-to- SiO_2 nanoparticles mass ratio, ball milling duration, and rotational speed. Additionally, the fiber addition content in the composite shell significantly impacts its mechanical performance. To systematically evaluate the effects of these factors, an orthogonal experimental design was implemented. Based on preliminary optimization trials, a four-factor, three-level orthogonal array (L₉ (4³)) was adopted, with the specific factors and level assignments detailed in Table 1.

2.3 Shell Preparation

The manufacturing process of the slurry is outlined in Table 3. To ensure the surface quality of castings, fibers were exclusively incorporated into the backing layer and seal layer. As depicted in Fig. 2, prior to preparing the backing layer, the treated fibers were dispersed in silica sol via ultrasonic agitation at 1200 W for 3 min to achieve homogeneous distribution. Subsequently, the filler was added according to the predetermined ratio and

following protocol: heated to 900°C at a rate of 5°C/min, held for 2 hours, and furnace-cooled to ambient temperature.

2.4 Microstructural Analysis of Treated Fibers and Their Dispersion Behavior in Silica Sol

2.4.1 Fiber Surface Morphology Analysis

The surface microstructure of treated fibers was



characterized using a Hitachi SU8220 field-emission scanning electron microscope (Hitachi Ltd., Japan) to evaluate the distribution uniformity of SiO₂ nanoparticles on fiber surfaces. To further verify the presence of hydroxyl (-OH) groups^[20] and investigate bonding mechanisms between nanoparticles and fibers, Fourier transform infrared (FTIR) spectroscopy was employed for functional group analysis.

2.4.2 Fiber Dispersion Analysis in Silica Sol

The attachment of SiO₂ nanoparticles onto fiber surfaces introduces hydroxyl groups, significantly enhancing the wettability between fibers and the silica sol. To quantify dispersion homogeneity, treated fibers ultrasonically dispersed in silica sol and transferred to Petri dishes for macroscopic observation. A grayscale entropy-based image analysis method (detailed in our prior study [21]) was applied to calculate dispersion entropy, enabling objective evaluation of fiber distribution uniformity. Notably, entropy values provide reliable dispersion metrics only under constant fiber loading conditions, as variations in fiber content induce grayscale information inconsistency across images, invalidating direct quantitative comparison. Consequently, fiber dispersion in silica sol was excluded from the orthogonal experimental evaluation criteria to ensure methodological rigor.

2.5 Shell Properties and Comprehensive Weighted Scoring Method

2.5.1 Bending Strength and High Temperature Self-load Deformation of the Shell

The tests for the bending strength and high temperature self-load deformation of the shell follow the industry standard HB5352.1-2004 and HB5352.2-2004. The shape and size of the specimens are shown in Fig. 2. The bending strength of the shell is tested using the TKW (Xiangtan Xiangyi Instrument Co., LTD.) shell high-temperature bending tester. The high-temperature bending strength needs to be tested after being reheated to 1200°C for 10 minutes. After the shell fractures, the surface microstructure of the shell fracture is observed using SEM (S-3400N) to analyze the interface bonding condition between the fibers and the matrix as well as the failure mode of the fibers during the fracture process. The high temperature self-weight deformation specimens need to be reheated to 1200°C after being baked and then measured after cooling in the furnac.



Table 1 Factors and Levels Affect	ing the Performance of the Shell
-----------------------------------	----------------------------------

Preparation factors	A: fiber: SiO ₂ (g: g)	B: ball rotational speed (r/min)	C: ball milling duration (min)	D: Fiber addition amount (% of the quality of filler)
Level 1	2:1	200	6	0.1
Level 2	1:1	300	10	0.15
Level 3	1:2	400	8	0.2

Table 2. Preparation of the shell

Coating Binder Fil		Filler (mesh)	Binder: filler (g: g)	Stirring method	Stucco sands (mesh)	Drying time (h)
Primary layer (1)		Zircon sand (325, Zhengzhou Honghu Chemical Co., Ltd., China)	1:3	Mechanical stirring for 24h (electric mixer, Hebei Shengxing Instrument Equipment Co., Ltd., China)	Zircon sand (100-120, Zhengzhou Honghu Chemical Co., Ltd., China)	12
Transition layer (2)	Silica sol (25%, Linyi Kehan Silicon	Mullite sand (200, Zhengzhou Honghu Chemical Co., Ltd., China)	1:1.6	Mechanical stirring for 12h (electric mixer, Hebei Shengxing Instrument Equipment Co., Ltd., China) Instrument Equipment Co., Ltd., China)	Mullite sand (30-60, Zhengzhou Honghu Chemical Co., Ltd., China)	24
Back layer (3,4)	Products Co., Ltd., China)	Mullite sand (200, Zhengzhou Honghu Chemical	1:1.4	Fiber: Steel fibers (added according to Table 1), the steel fibers are added into the silica sol and then ultrasonicated at 1200W	Mullite sand (16-30, Zhengzhou Honghu Chemical Co., Ltd., China)	24
Seal layer (5)		Co., Ltd., China)		power for 3 minutes, followed by stirring with refractory powder for 2 hours.		24

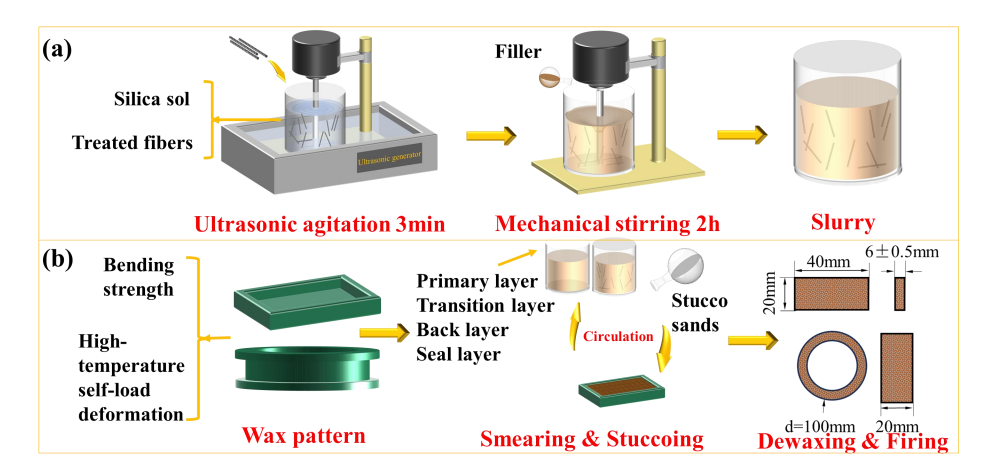


Fig. 2: Preparation process of slurries and shell: (a) Preparation of slurries; (b) Preparation of shell

2.5.2 Comprehensive Weighted Scoring Method

The comprehensive weighted scoring method is

used to evaluate the results obtained from orthogonal experiments, with a total score of 100 points set. The

scoring criteria are shown in Table 3. During the preparation of the shell, a good green bending strength can ensure that the shell does not break before and during the wax removal process. Another problem faced by the silica sol shell is its relatively low green bending strength, which is also the main issue that the reinforced shell aims to improve. Therefore, the weight coefficient of normal temperature bending strength is 0.4. In addition, the heat-resistant fibers still play a role at high temperatures, and the deformation of the shell at high temperatures will cause changes in the dimensional accuracy of the casting. Therefore, the deformation due to high-temperature self-weight is also relatively important. However, since the deformation amount due to high temperature self-load deformation needs to be kept low, the scoring criteria for this part adopt the method 1-high-temperature self-weight deformation amount for calculation.

3 Results and Discussion

3.1 Microstructural Characteristics of Treated Fibers

3.1.1 Fiber Surface Morphology

Fig. 3 compares the surface morphologies of untreated and treated fibers. As shown in Fig. 3(a), untreated fibers exhibit irregular surface grooves, which generate excessive interfacial friction and promote fiber entanglement during processing, thereby hindering uniform dispersion. In contrast, Fig. 3(b) demonstrates that SiO₂ nanoparticles (particle size: >15 nm) are successfully anchored onto treated fiber surfaces via mechanical coating. These nanoparticles partially fill the grooves. However, localized agglomeration of SiO₂ nanoparticles is observed due to van der Waals interactions and incomplete dispersion during ball milling.

3.1.2 FTIR Analysis of Fibers

The FTIR spectra of untreated and treated fibers are compared in Fig. 4. Distinct absorption peaks at 475 cm⁻¹, 807 cm⁻¹, and 1100 cm⁻¹ correspond to the bending vibration, symmetric stretching vibration, and asymmetric stretching vibration of Si-O-Si bonds. Respectively, confirming the successful deposition of SiO₂ nanoparticles on fiber surfaces and validating the feasibility of the mechanical coating technique. Additionally, the presence of hydroxyl (-OH) groups is evidenced by characteristic peaks at 3415 cm⁻¹ (O-H stretching vibration) and 1630 cm⁻¹ (O-H bending vibration. When fibers are incorporated into the silica sol, the Si-O-H groups on the fiber surfaces

interact with Si-O-H groups in the sol through a polycondensation reaction, releasing water molecules and forming Si-O-Si ether linkages, thereby enhancing fiber-matrix interfacial bonding. Concurrently, the introduced -OH groups improve the wettability between fibers and the silica sol.

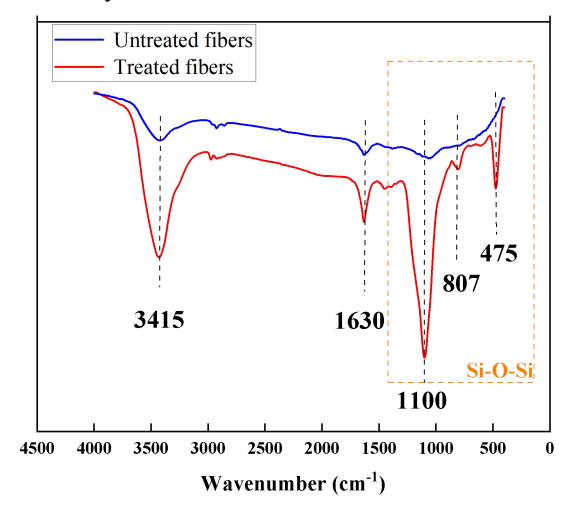


Fig. 4: Infrared spectra of the original fibers and the fibers after treatment

3.2 Influence of Processing Parameters on Fiber Dispersion in Silica Sol

The dispersion behavior of fibers treated under varying parameters in silica sol diverges significantly due to differences in SiO2 nanoparticles density on fiber surfaces and inter-fiber entanglement severity. FTIR analysis confirms that hydroxyl (-OH) groups introduced by nano-SiO2 particles enhance fiber-sol wettability. As shown in Figure 5, the image of fiber dispersion and Figure 6, the entropy values of the dispersion images, respectively, even at a low fiber loading of 0.1 wt%, dispersion homogeneity varies markedly across treatment protocols: prolonged ball milling durations and elevated speeds induce irreversible fiber entanglement during mechanical coating, which persists despite subsequent ultrasonic agitation, as exemplified by Sample 9. This degraded dispersion is quantifiable via entropy analysis of grayscale images, where Sample 9 exhibits a 34% lower entropy value than optimally treated fibers (Process 1). These findings underscore that dispersion quality is synergistically governed by surface hydroxylation (enhancing wettability) and mechanical processing parameters (controlling entanglement), with excessive milling energy paradoxically undermining dispersion despite improved nanoparticle adhesion, thereby necessitating parameter optimization to balance

interfacial chemistry and physical dispersion dynamics.

Table 3 Criteria for Shells' Performance Evaluation

NO.	Evaluation Project	Weight coefficient	Calculation method		
1	The green bending $strength(Y_1)$	0.4	The highest score among the results is designated as Y_{lmax} , while the others are designated as Y_{l} . The total score is: $(Y_{l}/Y_{lmax})\times0.4$		
2	The sintering bending strength (Y ₂)	0.15	The highest score among the results is designated as Y_{2max} , while the others are designated as Y_2 . The total score is: $(Y_2/Y_{2max})\times 0.15$		
3	The high-temperature bending strength $(Y_{3)}$	0.15	The highest score among the results is designated as Y_{3max} , while the others are designated as Y_3 . The total score is: $(Y_3/Y_{3max})\times 0.15$		
4	1- high temperature self-load deformation (Y_4)	0.30	The highest score among the results is designated as Y_{4max} , while the others are designated as Y_4 . The total score is:: $(Y_4/Y_{4max})\times 0.3$		

$$Y = \frac{Y_1}{Y_{1 \text{max}}} \times 0.4 \times 100 + \frac{Y_2}{Y_{2 \text{max}}} \times 0.15 \times 100 + \frac{Y_3}{Y_{3 \text{max}}} \times 0.15 \times 100 + \frac{Y_4}{Y_{4 \text{max}}} \times 0.3 \times 100$$
Note:

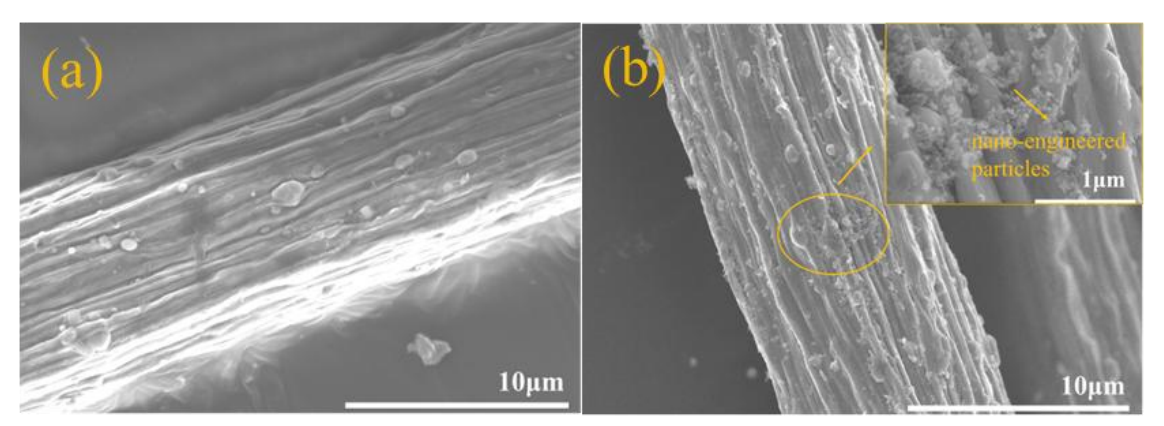


Fig. 3: Microscopic surface morphology of the fibers(a) untreated fiber; (b) treated fiber

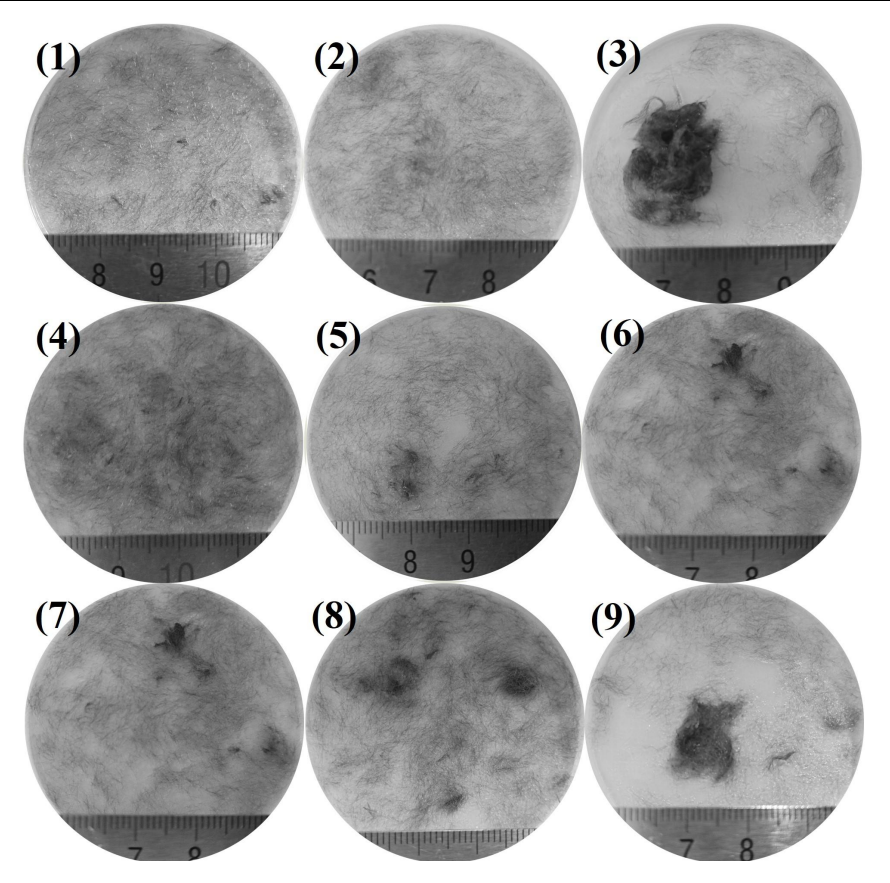


Fig. 5: Image of the dispersion of fiber in silica sol after orthogonal treatment (the serial numbers correspond to those in Table 2)

When the fiber addition content increases to 0.15 wt% (Fig. 5(2, 6, 7)), fibers remain predominantly dispersed in the silica sol with only minor localized agglomeration, attributable to the inverse correlation between ball milling speed and duration in the optimized parameter set: higher rotational speeds paired with shorter durations and lower speeds with extended durations synergistically minimize fiber entanglement during mechanical coating. Entropy analysis quantifies this behavior, identifying Process 2 as achieving peak dispersion homogeneity through balanced nanoparticle adhesion and fiber integrity. Conversely, at 0.2 wt% fiber loading (Fig. 5(3, 4, 8)), exhibits severe entanglement and agglomeration due to high-speed-induced fiber damage and insufficient time for nanoparticle redistribution, while Sample 4 maintains moderate dispersibility as prolonged low-energy milling reduces inter-fiber friction while ensuring sufficient nano-SiO2 attachment. These results highlight threshold-driven dispersion dynamics: at 0.15 wt%, optimized speed-duration pairs limit cumulative mechanical energy input to prevent entanglement, whereas at 0.2 wt%, higher fiber density amplifies entanglement risks, necessitating compensatory parameter adjustments to preserve dispersion. Entropy values quantitatively reflect the trade-off between nanoparticle coverage and fiber entanglement, with Process 2 exemplifying the equilibrium where interfacial chemistry and physical dispersion dynamics optimized.

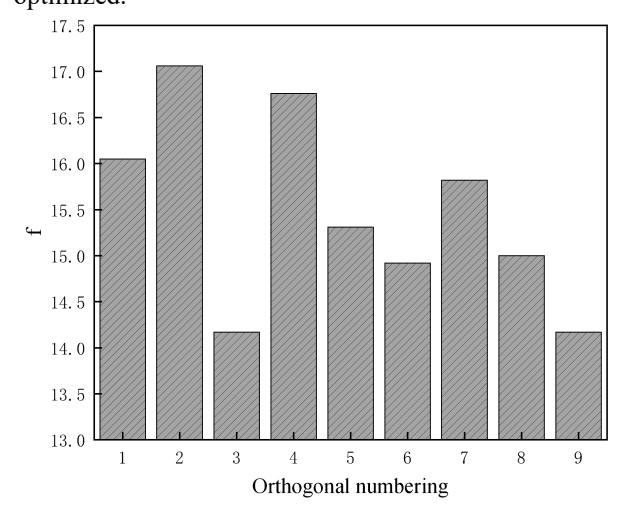


Fig. 6: Calculation of Entropy Value of Fiber Dispersion Image

33 Comprehensive Weighted Scoring Analysis Comprehensive Weighted Scoring Analysis

The orthogonal experimental matrix and corresponding results are summarized in Table 2. Range analysis of the data (Fig. 7) revealed that the significance order of influencing factors is D> B> A> C. The optimal parameter combination was identified as A2B3C2D2, corresponding to a 1:1 mass ratio of fibers to SiO₂ nanoparticles, ball milling speed of 400 rpm, ball milling duration of 10 min, and fiber addition content of 0.15 wt%. Shells fabricated with this optimized formulation exhibited a green bending strength of 3.76 MPa (86% increase compared to non-fiber-reinforced shells), sintering bending strength of 6.83 MPa (67% enhancement), high-temperature bending strength of 18.22 MPa, and high-temperature self-weight deformation of 0.52% (46% reduction versus conventional shells).

The influence of fiber addition content on shell performance is governed by two primary mechanisms: at a 0.1wt% loading, fibers exhibit uniform dispersion but provide insufficient reinforcement density, resulting in limited strength enhancement. Whereas a 0.2 wt% loading induces fiber agglomeration due to excessive inter-fiber friction, forming poorly wetted clusters that act as stress concentrators and interfacial defect.

Ball milling speed critically modulates surface treatment efficacy, where low speeds yield sparse nano-SiO₂ coverage due to insufficient kinetic energy for nanoparticle adhesion. While, high speeds promote fiber entanglement via intensified mechanical collisions, persisting even after ultrasonic dispersion, ultimately degrading shell performance through agglomerate formation. Similarly, ball milling duration exhibits threshold-dependent effects: shorter durations lead to incomplete surface modification, whereas prolonged milling exacerbates fiber damage and entanglement, with an optimal duration of 10 min achieving homogeneous nanoparticle distribution without compromising dispersibility. The fiber-to-nano-SiO2 ratio further dictates interfacial architecture, as excess nanoparticles form a discontinuous interfacial layer, whereas a balanced 1:1 ratio establishes a nanoparticle monolayer that maximizes bonding sites while minimizing agglomeration-driven defects. Collectively, these parameters exhibit interdependent threshold effects, necessitating balanced optimization to avoid performance degradation from over-processing.

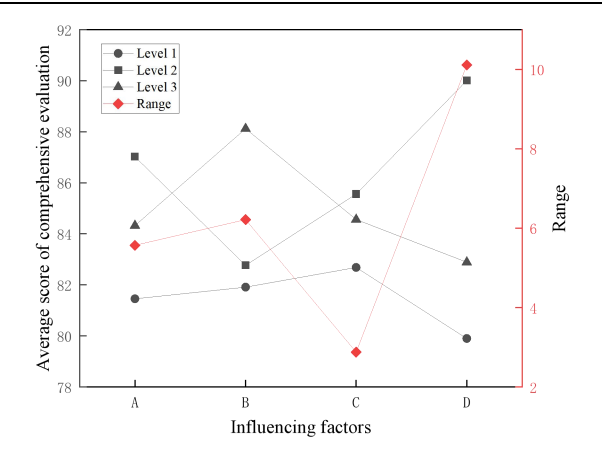


Fig. 7 Analysis of Variance for Orthogonal Experiments

3.4 Mechanism of Fiber Reinforcement in Shell

Fig. 8 illustrates the fracture surface morphology of the shell. As shown in Fig. 7(a), the presence of fibers effectively impedes crack propagation by forcing cracks to extend along the fiber-matrix interface, thereby

enhancing the shell's strength. During the drying process, SiO₂ nanoparticles on fiber surfaces polycondensation reactions with the silica sol matrix, forming robust interfacial bonds (Fig. 8(b)). Furthermore, Fig. 8(c) reveals that SiO₂ nanoparticles facilitate the formation of Silicon-oxygen chain anchored to fiber surfaces. These chains contribute to crack resistance by dissipating fracture energy through bond rupture (Fig. 8(d, e)). However, the growth mechanism of these siloxane chains remains to be elucidated, as this study did not identify conclusive evidence to explain their formation kinetics. Notably, the strong interfacial bonding enables efficient load transfer from the matrix to the fibers during mechanical failure, ultimately causing fiber fracture under applied stress (Fig. 8f). This fiber fracture behavior absorbs and redistributes fracture delaying catastrophic shell significantly improving overall strength.

Table 4 Orthogonal Table and Experimental Results

	Factors								
NO.	A/g : g	B/(r/min)	C/min	D/%	Y ₁ /MPa	Y ₂ /MPa	Y ₃ /MPa	Y4/%	Y
1	2:1	200	6	0.10	2.44	4.73	10.22	99.10	75.31
2	2:1	300	10	0.15	3.13	6.45	13.94	99.99	89.94
3	2:1	400	8	0.20	2.96	6.50	13.19	98.68	87.20
4	1:1	200	10	0.20	3.15	4.84	14.40	99.40	86.79
5	1:1	300	8	0.10	2.79	6.68	11.65	98.56	84.51
6	1:1	400	6	0.15	3.71	6.22	12.29	98.96	94.00
7	1:2	200	8	0.15	2.98	6.21	17.82	99.25	90.85
8	1:2	300	6	0.20	2.64	5.89	13.22	98.92	82.55
9	1:2	400	10	0.10	3.03	5.33	15.40	99.92	87.54
K1	252.45	252.95	251.86	247.36					
K2	265.30	257.00	264.28	274.79					
K3	260.94	268.74	262.55	256.55					
k1	84.15	84.32	83.95	82.45					
k2	88.43	85.67	88.09	91.60					
k3	86.98	89.58	87.52	85.52					
R	4.28	5.26	4.14	9.14					
Order of priority Optimal	18								
combinati on	$A_2B_3C_2D_2$				3.76				

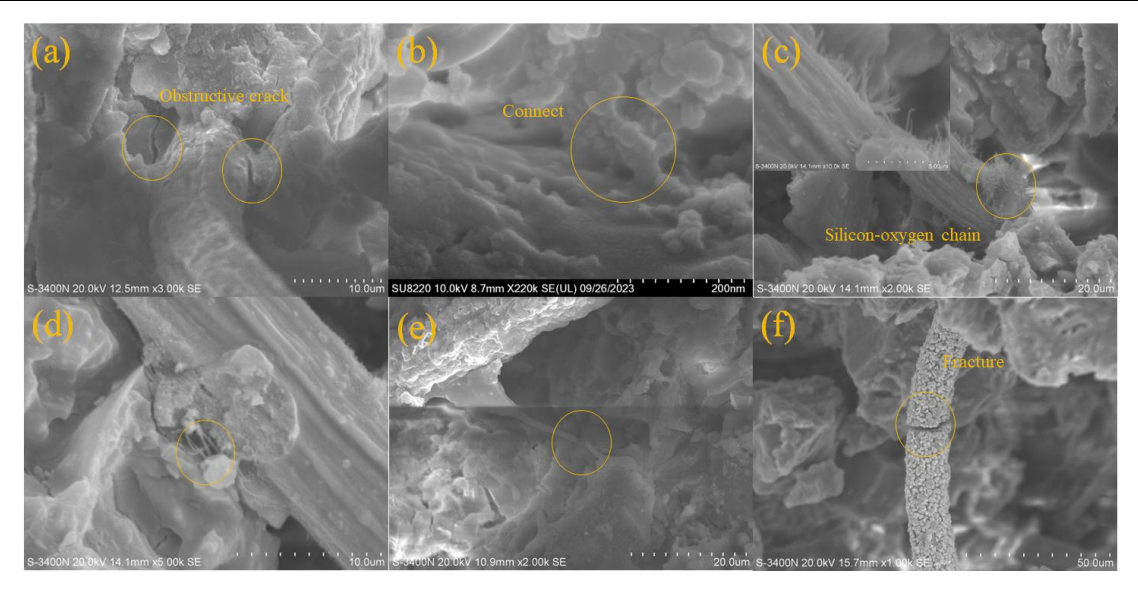


Fig. 8: Enhancement of Fibers in the Shell (a) hindering crack propagation; (b) connection between surface particles and matrix; (c) silicon-oxygen chains on the surface of fibers; (d) role of silicon-oxygen chains in fracture; (e) connection between silicon-oxygen chains; (f) fiber fracture

4. Conclusion

This study developed a novel fiber surface treatment method, investigating the functional groups and microstructural morphology of the fibers. An orthogonal experimental design was employed to optimize the processing parameters, followed by an evaluation of shell strength and high-temperature self-load deformation. The results demonstrated that:

- 1) When employing the mechanical coating method for fiber treatment, the optimized parameters are: a fiber-to-nano-SiO₂ weight ratio of 1:1, a ball milling speed of 400 rpm, and a ball milling duration of 10 minutes. With a fiber addition content of 0.15%, the shell achieves optimal performance. Under these conditions, the green bending strength of the shell reaches 3.76 MPa (an 86% improvement compared to fiber-free shells), while the sintering bending strength increases to 6.83 MPa (a 67% enhancement). The high-temperature bending strength attains 18.22 MPa, and the high-temperature self-load deformation is reduced to 0.52%.
- 2) The mechanical coating method effectively adheres nano-SiO₂ particles to fiber surfaces. These particles provide hydroxyl (-OH) groups that enhance fiber-silica sol wettability while also promoting the formation of Si-O-Si bonds through polycondensation between Si-O-H groups on the fiber surface and those in the silica sol, thereby strengthening fiber-matrix interfacial bonding. However, the growth mechanism of these Si-O-Si chains remains unresolved and requires

further

Acknowledgments

This work was supported by the National Natural Science Foundation of China, grant numbers 5186504; the University Science Foundation for Young Science and Technology Talents in Inner Mongolia Autonomous Region of China, grant numbers NJYT22078; Basic Scientific Research Expenses Program of Universities directly under Inner Mongolia Autonomous Region, grant numbers JY20220059; Inner Mongolia Autonomous Region 'Grassland Talent' project young innovative talent training program level I and Basic research expenses of universities directly under the Inner Mongolia Autonomous Region, grant numbers ZTY2023040.

Conflicts of Interest

We confirm that this work is original and has not been published elsewhere, nor is it currently under consideration for publication elsewhere. All the authors listed have approved the manuscript that is enclosed. No conflict of interest exits in the submission of this manuscript, and manuscript is approved by all authors for publication.

References

- [1] Pattnaik S, Karunakar D B, Jha P K. Developments in investment casting process-A review. Journal of Materials Processing Technology, 2012, 212(11): 2332-2348. https://doi.org/10.1016/j.jmatprotec.2012.06.003
- [2] Wei Y M, Lü Z G, Guo X. Influence of alkaline oxide on the deformation of ceramic shell mould at high

- temperatures during investment casting. Ceramics International, 2018, 44(17): 21197-21204. https://doi.org/10.1016/j.ceramint.2018.08.165.
- [3] Kumar S, Karunakar D B. Enhancing the permeability and properties of ceramic shell in investment casting process using ABS powder and needle coke. International Journal of Metalcasting, 2019, 13: 588-596. https:// doi.org/10.1007/s40962-018-00297-7.
- [4] Venkat Y, Choudary K R, Chatterjee D, et al. Development of mullite-alumina ceramic shells for precision investment casting of single-crystal high-pressure turbine blades. Ceramics International, 2022, 48(19): 28199-28106. https://doi.org/10.1016/j.ceramint.2022.06.124.
- [5] Znamenskii L G, Ivochkina O V, Varlamov A S. Acceleration of the formation on the sodium silicate binder in investment casting. Materials Science Forum, 2019, 4726(94): 673-677. https://doi.org/10.4028/www. scientific.net/MSF.946.673.
- [6] Harun Z, Kamarudin N H, Ibrahim M, et al. Reinforced green ceramic shell mould for investment casting process. Advanced Materials Research, 2015, 1087: 415-419. https://doi.org/10.4028/www.scientific.net/AMR.1087.41 5.
- [7] Li Z X, Liu X D, Lu Y, et al. Influence of rice husk on the properties of fiber-reinforced silicon sol shells used in investment casting process. Journal of Adhesion Science and Technology, 2021, 36(5): 469-489. https://doi.org/10.1080/01694243.2021.1926826.
- [8] Yuan C, Jones S. Investigation of fiber modified ceramic molds for investment casting. Journal of the European Ceramic Society, 2003, 23: 399-407. https://doi.org/10.1016/633 S0955-2219(02)00153-X.
- [9] Li Y F, Liu X D, Lü K, et al. Exploration on preparation process of high-strength fiber-reinforced shell for investment casting. International Journal of Metalcasting, 2021, 15: 692 – 699.
- [10] Lü K, Liu X D, Duan Z H. Effect of firing temperature and time on hybrid fiber-reinforced shell for investment casting. International Journal of Metalcasting, 2019, 13: 666 - 673. https://doi.org/10.1007/s40962-018-0280-x
- [11] Lü K, Shen S M, Ma C Q, et al. Research on modification of steel fiber in investment casting shell. International Journal of Metalcasting, 2022, 16: 1849-1857. https:// doi.org/10.1007/s40962-021-00722-4.

- [12] Lü K, Duan Z H, Liu X D, et al. Effects of fibre length and mixing routes on fibre reinforced shell for investment casting. Ceramics International, 2019, 45(6): 6925 6930. https://doi.org/10.1016/j.ceramint.2018.12.189.
- [13] Pattnaik S, Sutar K M. Enhancement of ceramic slurry rheology in investment casting process. Arabian Journal for Science and Engineering, 2021, 46(12): 1-12. https:// doi.org/10.1007/s13369-021-05834-x.
- [14] Gu Bo, Pu Guohong, Ding Bonan, et al. Improved interfacial bonding strength of silicone rubber/carbon fiber modified by dopamine. Polymer Composites, 2022, 43(10):6975-6986. https://doi.org/10.1002/pc.26759
- [15] Liu Zhen, Yang Yuxing, Bao Yongjie, et al. Strengthening the bonding interfaces of carbon reinforced aluminum laminate by slot structure. Polymer Composites, 2024, 45(11):9965-9976. https://doi.org/10.1002/pc.28451
- [16] Soonho Kim, Surak Choi, and Doo-Yeol Yoo. Surface modification of steel fibers using chemical solutions and their pullout behaviors from ultra-high-performance concrete. Journal of Building Engineering, 2020, 32: 101709. https://doi.org/10.1016/j.jobe.2020.101709
- [17] Liu J, Zhang B, Qi W, et al. Corrosion response of zinc phosphate conversion coating on steel fibers for concrete applications. Journal of Materials Research and Technology, 2020, 9(3):5912-5921. https://doi.org/10. 1016/j.jmrt.2020.03.117.
- [18] Liu T, Wei H, Zhou A, et al. Multiscale investigation on tensile properties of ultra-high performance concrete with silane coupling agent modified steel fibers. Cement and Concrete Composites, 2020, 111:103638. https://doi.org/10.1016/j.cemconcomp.2020.103638.
- [19] Du, S., Luan, C., Yuan, L. et al. Investigation on the effect of silane coupling agent treatment of steel fibers on the durability of UHPC. Archiv. Civ. Mech. Eng., 2023, 23(118). https://doi.org/10.1007/s43452-023-00667-x.
- [20] Naveen Kumar Kaliannan. Monte Carlo simulations of amorphous hydroxylated silica (SiO₂) nanoparticles. Computational Materials Science, 2017, 135:90-98. https://doi.org/10.1016/j.commatsci.2017.04.004.
- [21] Feng Zhicheng, Lv Kai, Jin Wenbo, et al. Preparation of steel fiber-reinforced shells for investment casting using ultrasonic-assisted dispersion. Journal of Adhesion Science and Technology, 2023, 37(11):1822-1836. https:// doi.org/10.1080/01694243.2022.2097578.